CCFE
CULHAM CENTRE FOR FUSION ENERGY

UK Atomic Energy Authority

UKAEA-CCFE-PR(22)13

H. Anand, D. Eldon, H. Q. Wang, G. McArdle, L. Pangione, M. Kochan

Assessment of the local expansion method for strike point position estimation for the MAST-Upgrade tokamak

Enquiries about copyright and reproduction should in the first instance be addressed to the UKAEA Publications Officer, Culham Science Centre, Building K1/0/83 Abingdon, Oxfordshire, OX14 3DB, UK. The United Kingdom Atomic Energy Authority is the copyright holder.

The contents of this document and all other UKAEA Preprints, Reports and Conference Papers are available to view online free at scientific-publications.ukaea.uk/

Assessment of the local expansion method for strike point position estimation for the MAST-Upgrade tokamak

H. Anand, D. Eldon, H. Q. Wang, G. McArdle, L. Pangione, M. Kochan

This is a preprint of a paper submitted for publication in Fusion Engineering and Design

Assessment of the local expansion method for strike point position estimation for the MAST Upgrade tokamak

H. Anand[1], D. Eldon[1], M. Kochan[2], G. McArdle[2], L. Pangione[2], and H.Q. Wang[1]

[1] *DIII-D National Fusion Facility, General Atomics, PO Box 85608, San Diego, CA 92186, USA*
[2] *Culham Centre for Fusion Energy, Culham Science Centre, Abingdon, OX14 3DB, United Kingdom*

Abstract

A local flux expansion method has been proposed for estimating the strike point position for the advanced divertor configuration on MAST Upgrade tokamak. The paper discusses the application and assesses the performance of the technique on a long-legged divertor plasma configuration on an operating device - the DIII-D tokamak. A comparison of the spatial location of the outer strike point estimated with the flux expansion method against the plasma boundary reconstruction and divertor diagnostics on DIII-D tokamak is reported. A good agreement with the equilibrium reconstruction and diagnostic data is achieved with respect to estimation of the spatial location of the outer strike point for the long-legged divertor plasma discharge.

Keywords— plasma control, flux expansion, strike point, divertor, reconstruction, real-time

1 Introduction

MAST Upgrade (MAST-U) tokamak [1] will explore extended- and expanded-leg divertor geometries, including the Super-X plasma configuration [2] (shown in figure 1), while allowing higher-performance core-plasma operations without excessive erosion and/or damage of the divertor target. Accurate real-time (RT) determination of the novel divertor magnetic field configuration, including spatial location of the divertor leg extension, will be required as an input to some proposed control systems. For example, a detachment control system using Langmuir probes[3] would need to know which probe(s) to read depending on the

strike point position at any given time. Several approaches have been considered already for real-time equilibrium reconstruction [4, 5, 6]. They consists in identifying, from experimental measurements, a distribution of the plasma current density that satisfies the pressure balance constraint and provide an accurate determination of the plasma shape and the divertor parameters. However, their application to exotic divertor configuration, especially long-legged divertors, for strike point estimation in MAST-U may be inaccurate. The inaccuracy can be hypothesized due to the fact that the equilibrium solvers are accurate in the plasma vicinity and are prone to errors far from the plasma. In addition, the MAST-U hosts passive stabilization plates [7] for vertical stability between the confined plasma and the super-X strike point, which may result in additional error in the spatial location of the divertor leg as estimated from established equilibrium reconstruction methods. A local higher order expansion of poloidal flux calculations constrained by the vacccum field equation, fitted to the local field and flux measurements is found to provide an accurate RT estimation of the plasma parameters in the vicinity of the measurements for JET and EAST tokamak [8, 9]. Thus, the local poloidal expansion method is a strong candidate for providing fast and reliable estimation of outer strike point for the advanced divertor configuration on the MAST-U tokamak.

This paper describes the implementation and benchmarking of the local poloidal flux expansion method developed for MAST-U on an operating device – the DIII-D tokamak. Section 2 introduces the fundamental concepts of the local poloidal flux expansion method. The implementation of the method on a long-legged DIII-D divertor plasma discharge type and the comparison with the offline and RT plasma boundary reconstruction and divertor diagnostics is discussed in Section 3. A brief overview of the method, implementation and results, as well as an outlook for the physics applications of the local poloidal flux expansion method to advanced divertor plasma configurations is provided in Section 4.

To avoid confusion with the term "flux expansion", commonly used to mean the change in spacing between flux surfaces at the divertor relative to the spacing at the plasma's midplane, we will refer to the local poloidal flux expansion method as "flux projection" for the rest of the paper.

2 The local poloidal flux expansion method

The local poloidal flux expansion method, or "flux projection" to avoid confusion, utilizes 6^{th} order expansions of the poloidal flux function, constrained by the vacuum field equations. The local field and flux measurements are then fitted to provide an accurate determination of the plasma shape and divertor parameters in the vicinity of the measurements. The formulation of the expansion is given as follows [8]:

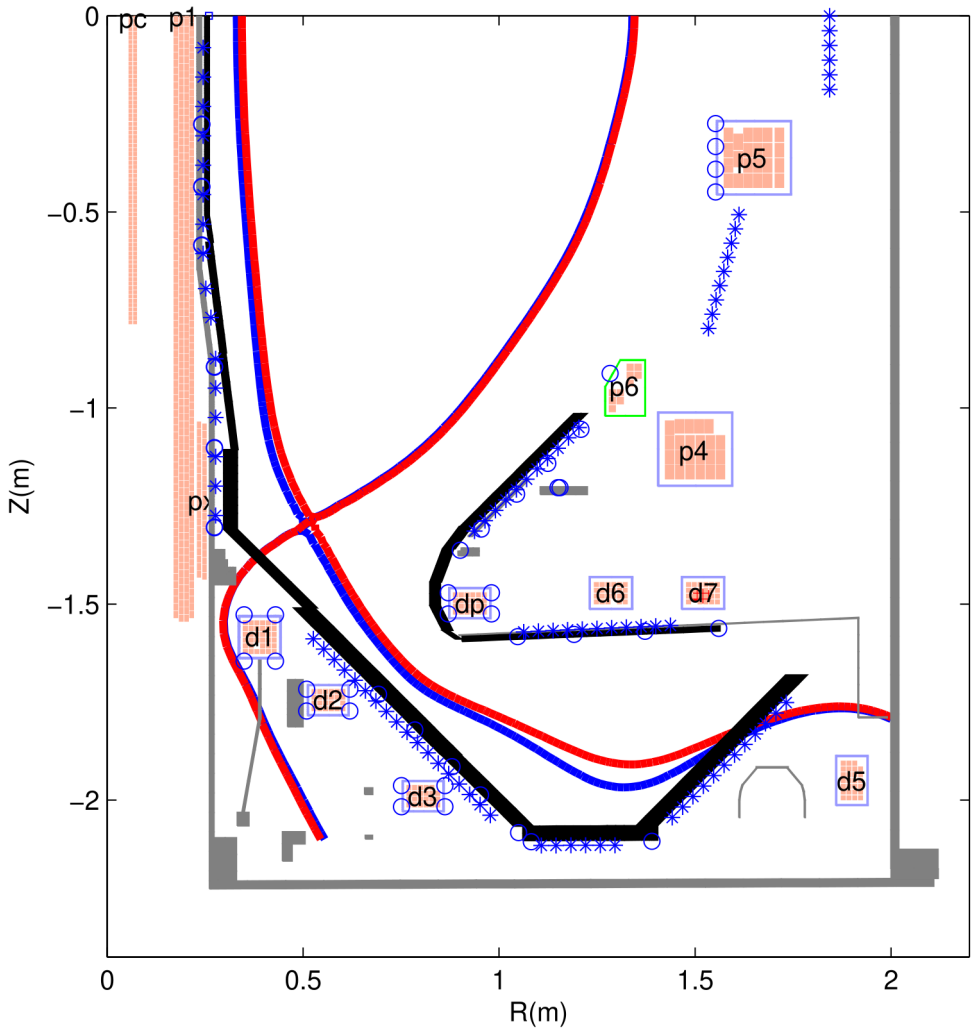

Figure 1: An example super-X divertor configuration in MAST-U. The magnetic probes are shown as blue crosses and flux loops are the circles. Coils are as labelled, vessel structure is grey. A hypothetical best estimate for the true separatrix position is given by the red curve, compared to a hypothetical result from flux projection in blue, with some error between them.

$$\psi(R,Z) = \sum_{\substack{i=0 \\ j=0 \\ i+j\leq 6}}^{6} a_{ij}\rho^i z^j \tag{1}$$

where, $\rho = R^2 - R_0^2$, $z = Z^2 - Z_0^2$ and (R_0, Z_0) is the center point of expansion. The coefficients of expansion, a_{ij} are determined by imposing the vacuum magentic field equation (2) and by fitting to the local flux and magnetic field measurements.

$$\Delta^* = 0; \Delta^* = \partial_{RR} + \partial_{ZZ} - \frac{1}{R}\partial_R \tag{2}$$

The 6th-order expansion leads to 13 independent coefficients to be determined. The poloidal flux and magnetic field can be written in terms of these coefficients as follows:

$$\begin{aligned} \psi_e(R,Z) &= \sum_{i=1}^{13} \psi_i(\rho,z)C_i \\ B_e(R,Z) &= \sum_{i=1}^{13} B_i(\rho,z)C_i \end{aligned} \tag{3}$$

where, ψ_e and B_e are the estimated values of the flux and field at R_j, Z_j. The coefficients, C_i are obtained by minimizing equation:

$$\chi^2 = \frac{1}{2}\sum_{Flux\ \ Loops} \big(\psi_m(j) - \psi_e(j)\big)^2 + \frac{1}{2}\sum_{Magnetic\ probes} \big(B_m(j) - B_e(j)\big)^2 \tag{4}$$

where, ψ_m and B_m are the measured values of the flux and field at R_j, Z_j. The Equation (4) can further be simplified in the following form:

$$\chi^2 = \frac{1}{2}\sum_{j=1}^{N_m} \big(m_j - \sum_{i=1}^{13} d_{ji}C_i\big)^2 \tag{5}$$

where, $m_j \equiv \psi_m, B_m$ are the measurements, $d_{ji} \equiv \psi_i(\rho_j, z_j), B_i(\rho_j, z_j)$ and N_m is the number of measurements. The minimization can be summarized as:

$$D\vec{C} = \vec{M} \tag{6}$$

where, $D_{ki} = \sum_{j=1}^{N_m} d_{ji}d_{jk}$ and $M_k = \sum_{j=1}^{N_m} d_{jk}m_j$, respectively. In the presence of active coils inside the vacuum region, the flux projection method requires measurements from which the contribution of the coils have been removed. These contributions are then added back to the flux reconstruction later. Complete details about the method can be found in [8, 9].

For the work presented in the paper, the flux projection method is applied for the determination of the poloidal fluxes on the DIII-D divertor contour using

the nearby magnetic sensors. The spatial location of the strike point is then estimated by selecting the location on the divertor contour corresponding to the poloidal flux closest to the X-point poloidal flux. However, at first an accurate estimation of outer strike point is performed using the offline equilibrium reconstruction and Langmuir Probe (LP) diagnostic data. The estimation from the flux projection method and real-time equilibrium reconstruction is then compared against the accurate estimation of the strike point derived from the offline equilibrium reconstruction and LP data analysis.

3 Implementation and comparison with equilibrium reconstruction code on DIII-D

The main operational parameters of the DIII-D tokamak are the following: typical major radius 1.69 m, typical minor radius 0.60 m, vacuum toroidal field up to 2.2 T, plasma current up to 2 MA, elongation up to 2.0 [10]. DIII-D also hosts a flexible poloidal-field coil system that allows tests with long-legged divertors. The magnetic diagnostic system of the DIII-D tokamak includes approximately 250 inductive sensors of various types: axisymmetric poloidal flux loops, diamagnetic-flux loops, magnetic probes and saddle loops for the measurement of local magnetic field, and Rogowski loops [11]. The extensive set of magnetic sensors, extreme shaping versatility and the presence of the Grad-Shafranov equilibrium reconstruction code, EFIT [12] and its RT version, EFITRT [4] sets a strong foundation for benchmarking the local poloidal flux expansion algorithm for strike point location estimation developed for MAST-U on DIII-D tokamak.

The performance of the flux projection method is checked on a DIII-D long-legged divertor plasma discharge, # 147740 (Figure 2(a)), involving a variation in radial placement of the outer divertor strike point, R_{OSP}, ranging from 1.20 m to 1.61 m (Figure 2(b)). The location of the flux loops and magnetic probes used by the flux projection method are shown in Figure 2(a). The evolution of the R_{OSP} and ψ_X from EFIT01 and EFITRT1 is shown in Figure 2(b,c). EFIT01 and EFITRT1 refers to the standard version with default parameter settings of EFIT and EFITRT, respectively. Differences in various plasma parameters between EFIT01 and EFITRT1 are expected and the reasons are discussed in [4].

The position of the strike point can be verified using profiles from Langmuir probe measurements (locations are shown in Figure 2(d)). These profiles are easiest to form during strike point sweeps, where the motion of the strike point (Figure 2(b)) fills in the profile. Referring to the floor and shelf regions marked in Figure 2, Langmuir probe arrays cover the ranges $1.207 \leq R \leq 1.352$ m on the floor and $1.500 \leq R \leq 1.696$ m on the shelf. Assuming that the standard, automatically generated EFIT01 results gives the strike point position to within a few cm and allowing for some padding, shot 147740 takes the strike point past both arrays and the relevant time ranges for obtaining good probe measurements

during sweeping are $2.5 < t < 3.1$ and $4.2 < t < 5$ s. These time-ranges can be subdivided into smaller intervals, each long enough for the strike point to move from one probe to the next, to test for different systematic errors in EFIT01's strike point position at different positions (when the strike point is near different magnetic probes).

Figure 3 shows a sample profile of probe data plotted against $R - R_{osp,EFIT01}$; the strike point should be at 0 if EFIT01 is performing perfectly. We can estimate the actual position of the strike point position from landmarks in the floating potential ϕ_f profile and from Eich fits [13] to heat flux and J_{sat} profiles. The eich fit is designed for heat flux, but the shape is empirically similar to the J_{sat} profile and the arguments behind its terms seem sensible, so it serves as a basis for strike point position estimation. The ϕ_f profile should have an inflection point at the separatrix [**?**]. This is typically located very close to a zero-crossing, and zero-crossings are easier to locate in noisy data. The locations of both landmarks for each ϕ_f profile has been estimated by manual inspection, with uncertainty in position based on scatter in the data (approximately the width of the band of scattered data for zero-crossings).

Figure 4 shows the corrections from several profiles. The direct uncertainty (red) from the estimates is increased (blue) to account for the 4 mm width of the probe tips [14]. With this in mind, the ϕ_f zero-crossing and inflection point methods provide essentially no correction, and neither does the Eich fit to J_{sat}. The fits to $q_{\|}$ suggest a correction of up to 3.8±2.2 mm, but the average correction from the slices considered is 2.5±2.0 mm. The average corrections indicated by the ϕ_f zero-crossing, ϕ_f inflection point, and J_{sat} Eich fit methods are 0.3±2.2, 0.5±0.7, and 0±0.2 mm. The ϕ_f methods suggest an increasing correction with time, but the uncertainty also increases. Taken together, these results do not confidently suggest a meaningful correction to EFIT01 for this shot and its reported strike point position should be taken as the best estimate for the true strike point position. This is consistent with past experience: EFIT01 typically agrees well with the Langmuir probes in the lower half of the machine [15]. It is also typical for EFITRT1 (the primary set of standard results from RTEFIT) and EFIT01 to disagree by ≈ 1 cm [15].

The flux projection method was applied to the DIII-D plasma discharge shown in Figure 2(a) for the determination of poloidal flux on the divertor contour, ψ_{div}. Using the DIII-D geometrical description of the divertor contour, flux loops and magnetic probes, the coefficient matrix, D is determined with the help of Equation (6). The full analytic form of the coefficient matrix can be found in [9]. Furthermore, ψ_X from EFITRT1 is used for the estimation of R_{OSP} in the flux projection method. In general, R_{OSP} from equilibrium reconstruction and flux projection method is obtained by selecting the spatial location where ψ_{div} is closest to the ψ_X.

Taking EFIT01 as nominal, the difference in the performance of EFITRT1 and the projection method is found by comparing the estimation of ψ_{div} and R_{OSP} relative to EFIT01 values is shown in Figure 5. Figure 5(a) shows a small

variation in the root mean square deviation (RMSD) of ψ_{div} between EFITRT1 vs. flux projection (both relative to EFIT01), thereby demonstrating a similar performance with respect to the estimation of ψ_{div}. As would be expected based on the agreement in ψ_{div} values, EFITRT1 and flux projection agree well on R_{OSP} as well (Figure 5(b,c)).

4 Summary and outlook

Tests using a DIII-D shot with a very long divertor leg indicate that flux projection can work as well as real-time equilibrium reconstruction, but no advantage in accuracy was found in DIII-D. DIII-D lacks passive stabilizing plates between the confined plasma and the strike point and so it cannot test the hypothesis that these plates may degrade accuracy of the equilibrium reconstruction in the divertor box in MAST-U. These plates should either give flux projection an accuracy advantage over real-time equilibrium reconstruction or have no effect. Either way, flux projection is fast to calculate and already implemented (as LEMUR [16]) in MAST-U, giving it advantages over EFITRT so far. Since flux projection is likely to provide good the strike point position with good accuracy in real-time, detachment control systems for MAST-U can be designed with this in mind.

Acknowledgement and Disclaimer

Acknowledgement:
This material is based upon work supported by the U.S. Department of Energy, Office of Science, Office of Fusion Energy Sciences, under Award(s) DE-SC0018991.

This work has been partly funded by EPSRC Grant is EP/T012250/1

Disclaimer: This report was prepared as an account of work sponsored by an agency of the United States Government. Neither the United States Government nor any agency thereof, nor any of their employees, makes any warranty, express or implied, or assumes any legal liability or responsibility for the accuracy, completeness, or usefulness of any information, apparatus, product, or process disclosed, or represents that its use would not infringe privately owned rights. Reference herein to any specific commercial product, process, or service by trade name, trademark, manufacturer, or otherwise does not necessarily constitute or imply its endorsement, recommendation, or favoring by the United States Government or any agency thereof. The views and opinions of authors expressed herein do not necessarily state or reflect those of the United States Government or any agency thereof.

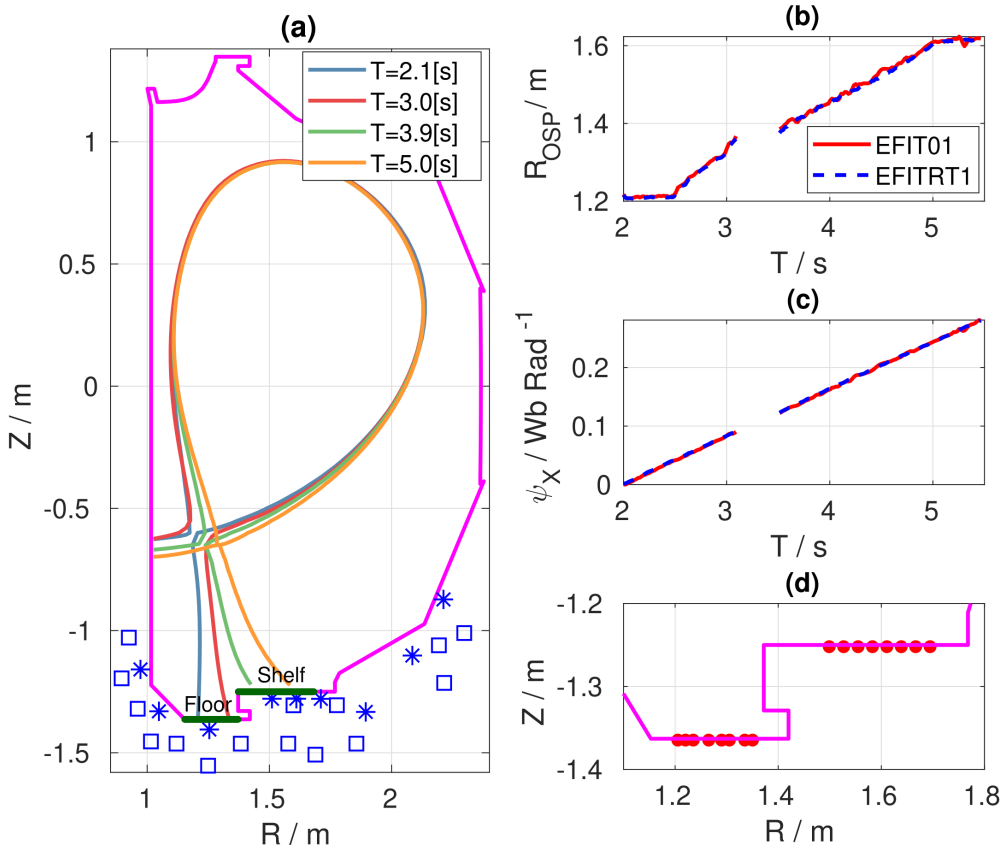

Figure 2: (a) Plasma magnetic equilibria from EFIT01 for #147740 at various time instants. The blue squares and stars give the position of the flux loops and magnetic probes and the solid dark green line denotes the part of the divertor contour used by local poloidal flux expansion method. Time evolution of: (b) radial position of the outer strike point, R_{OSP} and (c) poloidal flux at the separatrix, ψ_X from EFIT01 and EFITRT1. (d) Zoomed view of the divertor region with the Langmuir probe arrays shown as red filled circles. The empty region between the time interval 3.1 s - 3.5 s denotes the transition of the plasma equilibrium from the floor to the divertor shelf and is not accounted in the analysis.

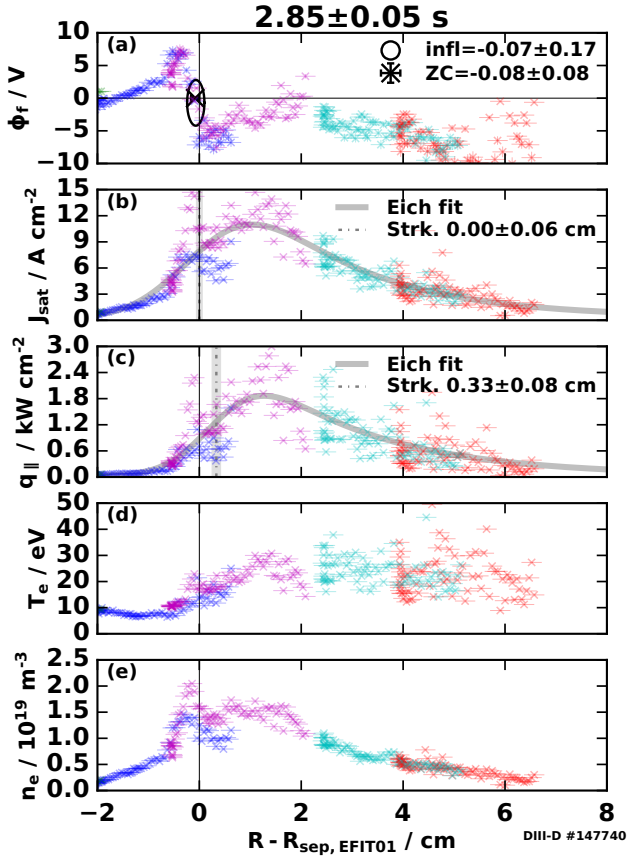

Figure 3: Profiles of LP measurements, plotted relative to EFIT01's strike point position, used to estimate a correction to EFIT01's strike point position. Colors correspond to different physical probes. The ϕ_f profile (a) has an X marking the estimated zero-crossing point, and an ellipse marking the estimated inflection point location. The J_{sat} (b) and $q_{\|}$ (c) plots are overlaid with a dash-dotted black line and gray band representing the strike point position given by Eich's function [13], with the function itself shown with gray curves. T_e (d) and n_e (e) are provided for reference.

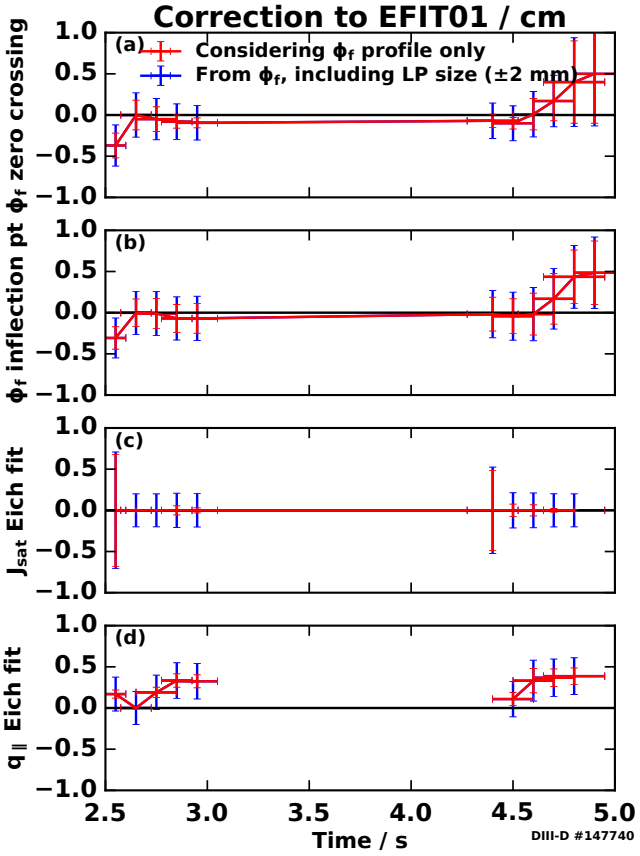

Figure 4: Corrections to EFIT01 vs. time, using various methods: the manually estimated zero-crossing of Langmuir probe ϕ_f profiles to define the true strike point position (a), manually estimated inflection point of the ϕ_f profile (b), Eich [13] fits to J_{sat} (c), and Eich fits to heat flux (d). The LPs have 4 mm wide tips [14], so 2 mm error has been added in quadrature with other errors.

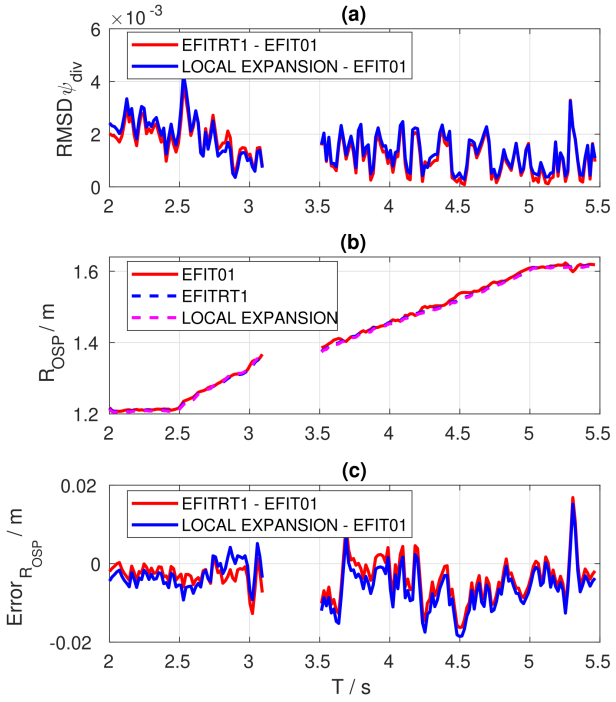

Figure 5: (a) Evolution of the RMSD of ψ_{div} between EFIT01 and EFITRT1 Vs. EFIT01 and the flux projection method. (b) Evolution of R_{OSP} from EFIT01, EFITRT1 and flux projection. (c) Evolution of the absolute error between EFIT01 and EFITRT1 Vs. EFIT01 and flux projection. The empty region between the time interval 3.1 s - 3.5 s denotes the transition of the plasma equilibrium from the floor to the divertor shelf and is not accounted in the analysis.

References

[1] Fishpool G, Canik J, Cunningham G, Harrison J, Katramados I, Kirk A, Kovari M, Meyer H and Scannell R 2013 *Journal of Nuclear Materials* **438** S356–S359 ISSN 00223115 URL http://dx.doi.org/10.1016/j.jnucmat.2013.01.067

[2] Valanju P M, Kotschenreuther M, Mahajan S M and Canik J 2009 *Physics of Plasmas* **16** ISSN 1070664X URL http://dx.doi.org/10.1063/1.3110984

[3] Guillemaut C, Lennholm M, Harrison J, Carvalho I, Valcarcel D, Felton R, Griph S, Hogben C, Lucock R, Matthews G F, Thun C P V, Pitts R A, Wiesen S and JET contributors 2017 *Plasma Phys. Control. Fusion* **59** 045001

[4] Ferron J R, Walker M L, Lao L L, John H E, Humphreys D A and Leuer J A 1998 *Nuclear Fusion* **38** 1055–1066 ISSN 0029-5515 URL http://stacks.iop.org/0029-5515/38/i=7/a=308

[5] Moret J M, Duval B P, Le H B, Coda S, Felici F and Reimerdes H 2015 *Fusion Engineering and Design* **91** 1–15 ISSN 09203796 URL //www.sciencedirect.com/science/article/pii/S0920379614005973

[6] Gates D A, Ferron J R, Bell M, Gibney T, Johnson R, Marsala R J, Mastrovito D, Menard J E, Mueller D, Penaflor B, Sabbagh S A and Stevenson T 2005 *Nuclear Fusion* **46** 17–23 ISSN 0029-5515 URL http://stacks.iop.org/0029-5515/46/i=1/a=002

[7] Milnes J, Ayed N B, Dhalla F, Fishpool G, Hill J, Katramados I, Martin R, Naylor G, O'Gorman T and Scannell R 2015 *Fusion Engineering and Design* **96-97** 42–47 ISSN 09203796 URL http://dx.doi.org/10.1016/j.fusengdes.2015.03.002

[8] O'Brien D P, Ellis J J and Lingertat J 1993 *Nuclear Fusion* **33** 467–474 ISSN 00295515

[9] Guo Y, Xiao B and Luo Z 2011 *Plasma Physics and Controlled Fusion* **53** ISSN 07413335

[10] Luxon J L 2002 *Nuclear Fusion* **42** 614–633 ISSN 00295515

[11] Strait E J 2006 *Review of Scientific Instruments* **77** ISSN 00346748

[12] Lao L L, St John H E, Peng Q, Ferron J R, Strait E J, Taylor T S, Meyer W H, Zhang C and You K I 2005 *Fusion Science and Technology* **48** 968–977 ISSN 15361055

[13] Eich T, Sieglin B, Scarabosio A, Fundamenski W, Goldston R, Herrmann A and ASDEX Upgrade Team 2011 *Phys. Rev. Lett.* **107** 215001

[14] Watkins J G, Taussig D, Boivin R L, Mahdavi M A and Nygren R E 2008 *Rev. Sci. Instrum.* **79** 10F125

[15] Eldon D, Hyatt A, Covele B, Eidietis N, Guo H, Humphreys D, Moser A, Sammuli B and Walker M 2020 *Fusion Engineering and Design* **160** 111797

[16] McArdle G, Pangione L and Kochan M 2020 *Fusion Engineering and Design* **159** 111764 ISSN 0920-3796